

Tuning Protein Frameworks *via* Auxiliary Supramolecular Interactions

Sylvain Engilberge,¹ Martin L. Rennie,¹ Elise Dumont,² Peter B. Crowley*¹

¹School of Chemistry, National University of Ireland, University Road, Galway, H91 TK33, Ireland

²Université de Lyon, École Normale Supérieure de Lyon, CNRS, Université Claude Bernard Lyon 1, Laboratoire de Chimie, UMR 518, F-69342 Lyon, France

*Correspondence to:

peter.crowley@nuigalway.ie

+353 91 49 24 80

Published as: <https://pubs.acs.org/doi/10.1021/acsnano.9b04115>

Abstract

Protein crystals with their precise, periodic array of functional building blocks have potential applications in biomaterials, sensing and catalysis. This paper describes how a highly-porous crystalline framework of a cationic redox protein and an anionic macrocycle can be modulated by a small cationic effector. Ternary composites of protein (~13 kDa), calix[8]arene (~1.5 kDa) and effector (~0.2 kDa) formed distinct crystalline architectures, dependent on the effector concentration and the crystallization technique. A combination of X-ray crystallography and DFT calculations was used to decipher the framework variations, which appear to depend on a calixarene conformation change mediated by the effector. This “switch” calixarene was observed in three states, each of which is associated with a different interaction network. Two structures obtained by co-crystallization with the effector contained an additional protein “pillar”, resulting in framework duplication and decreased porosity. These results suggest how protein assembly can be engineered by supramolecular host – guest interactions.

Keywords

biomaterials, macrocycle, molecular switch, self-assembly, spermine

Controlled protein assembly provides a means to construct biocompatible, nanoscale devices and functional materials.¹⁻⁵ Porous assemblies are particularly attractive considering their applications in storage, delivery and catalysis.⁶⁻⁹ To date, specific protein architectures including nanocages have been generated from self-assembling building blocks with engineered interfaces. Crystalline architectures, characterized by highly-ordered three dimensional arrays and in some cases nanoscale porosity, are also well-studied.^{2,7,10-19} Although crystallogenesis can be a bottleneck, this special case of protein assembly provides detailed structural insights that aid design. Ligands that facilitate protein assembly and crystallization have emerged as game-changers in the elaboration of crystalline assemblies.^{14,17,20-30} Such “molecular glues” trigger assembly by providing a surface on which two or more proteins can associate (Figure 1). Importantly, the choice of glue can yield different protein architectures.^{22,29,30}

We have demonstrated controlled assembly of cationic proteins by anionic macrocycles such as sulfonato-calix[n]arene (**sclx_n**).^{22,29-31} Our focus is on the lysine-rich cytochrome *c* (cytc), a redox active building block that is applied widely in biosensor development.^{32,33} Previously, we reported auto-regulated assembly of cytc by **sclx₈**.^{29,31} At ~1 eq. **sclx₈**, cytc forms a tetramer. At >3 eq. **sclx₈**, the tetramer disassembles to form calixarene-coated monomers. X-ray crystallography revealed corresponding oligomers in the solid state with distinct crystal forms that depend on the protein:ligand ratio. A highly-porous crystalline framework (85 % solvent content) was obtained at >3 eq. **sclx₈** (PDB 6gd9, Figure 1).²⁹ This lattice exists exclusively due to **sclx₈**, which mediates all of the crystal contacts. Adopting either the pleated loop or double cone conformations,^{29,34,35} **sclx₈** occurs sandwiched between cytc monomers providing the necessary “glue” to support the framework. A third calixarene does not participate directly in the framework but is solvent exposed and faces into the crystal voids. These “switch” calixarenes are ~3 nm apart, which is approximately the diameter of cytc, while the longest distance between framework laterals is ~12 nm (Figure 1). Consequently, the crystal voids are sufficiently large to accommodate additional components. This observation suggested the possibility that the framework might be augmented with additional building blocks.

In the present work, we began by targeting the double cone conformation of **sclx₈** as a site for crystal engineering. The calixarene cavities inspired us to perform host – guest supramolecular chemistry in the crystals. Tetracationic spermine (**spr**) was chosen as the guest molecule for three reasons. (1) **spr** is a known modulator of biomolecular structures;^{14,36-39} (2) polycationic amines are well-established calixarene binders;^{34,40} and (3) **spr** is structurally analogous to the di-lysine motif (Figure S1), which occurs frequently in cytc – calixarene interfaces.^{28,29} Competition between cytc and **spr** for **sclx₈** binding in solution was confirmed by NMR experiments. Co-crystallization of

ternary mixtures of *cytc*, **sclx₈** and **spr** yielded two different architectures, which appear to depend on **sclx₈** – **spr** complexation, as evidenced by crystal structure analysis and DFT calculations. This first study demonstrates crystalline framework modulation by using auxiliary supramolecular interactions.

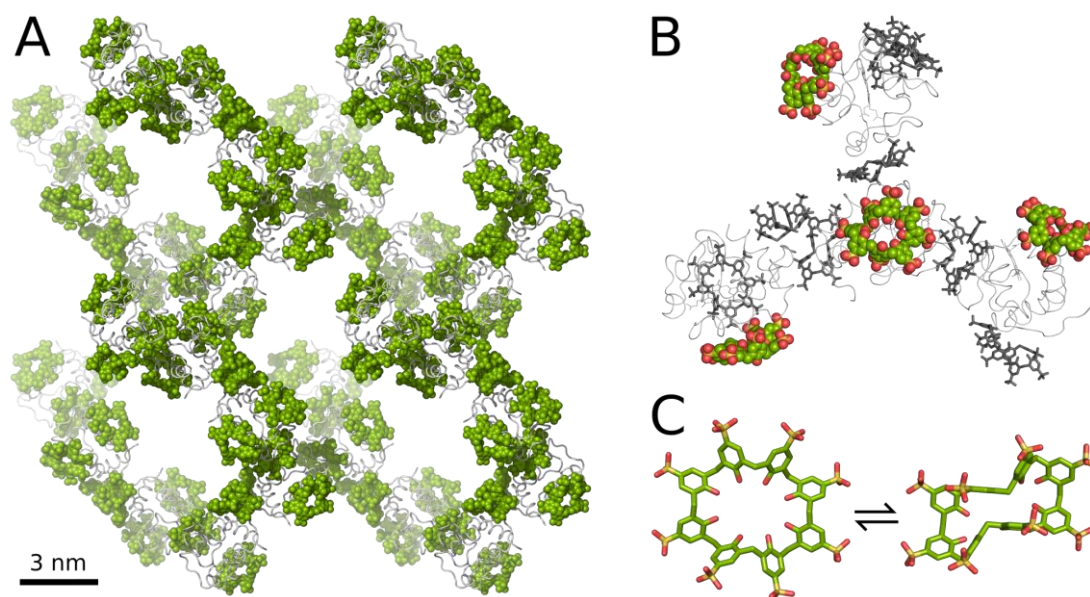


Figure 1. (A) The previously reported *cytc* – **sclx₈** framework obtained at >3 eq. calixarene (PDB 6gd9) has nanoscale porosity and no protein – protein contacts.²⁹ Protein and ligand are shown in grey ribbon and green spacefill, respectively. (B) The core assembly unit, with four molecules of *cytc* and crystal contacts *via* the calixarene “glue” (grey sticks). The “switch” calixarene (spacefill) does not participate in crystal contacts. (C) The pleated loop and double cone conformations of **sclx₈**.

Results

Solution state analysis of cytc – sclx₈ – spr interactions. Previously, using NMR spectroscopy and isothermal titration calorimetry, we characterized in detail the auto-regulated assembly of cytc by sclx₈.^{29,31} In brief, the HSQC spectrum of cytc is broadened beyond detection at ~1 eq. sclx₈ due to tetramer formation. At ~3 eq. sclx₈, the HSQC signals of cytc reappear consistent with the formation of calixarene-coated monomers.²⁹ Here, we monitored the effects of spr in ternary mixtures with sclx₈ and cytc. The data indicate that spr competes with cytc for sclx₈ complexation (Figure S2). Approximately 8 eq. spr were sufficient to liberate cytc from complexation with sclx₈, at the low salt conditions of the NMR experiments. The relatively high eq. spr required for competition reflects the high lysine content of cytc (16 x lys) compared to 4 amines in spr. Furthermore, in contrast to the linear spr, the protein provides extended surfaces for tighter interactions with the calixarene.

Optimization of cytc – sclx₈ co-crystals. Previously, cytc – sclx₈ co-crystals were obtained in space group *P4₃2₁2* (PDB 6gd9) with 3 - 12 eq. sclx₈ and ~2 M ammonium sulfate.²⁹ These ovoid crystals diffracted weakly (2.7 Å) and were prone to twinning. Here, the crystal quality was improved by using ≥ 20 eq. sclx₈, which resulted in a “diamond” morphology (Figure 2) in 3 to 7 days. A dataset collected to 2.5 Å resolution revealed the identical space group but better diffraction properties than reported before. The crystal packing was also identical, within error. For simplicity, this crystal is referred to as structure **0**. Interestingly, a significant backbone conformation change of cytc is evident.⁴¹ Residues 79 - 82 are displaced from their native positions (C^α RMSD ~1.5 Å) and Met80 no longer coordinates the heme (Figure S3).

Crystal soaking. Experiments were performed on cytc – sclx₈ co-crystals to test the effect of spr interactions with calixarenes already bound to cytc. Crystals were soaked in their respective crystallization condition supplemented with 50 - 200 mM spr for up to five minutes. There was no visible degradation of the crystals in this timeframe suggesting that the crystals were stable despite the high spr concentration. The soaked crystal form is referred to as structure **I**.

cytc – sclx₈ – spr ternary co-crystallization. To explore further the effects of spr we performed co-crystallization experiments with ternary mixtures of 2 mM cytc, 20 - 40 mM sclx₈ and 10 - 100 mM spr (Figure 2). Low concentrations of spr (10 or 20 mM) resulted in ~5-fold larger crystals that grew in 7 days. A metastable zone occurred at 30 mM spr, crystals grew slower and a notable change in

morphology was observed in some crystallization drops. This crystal morphology is referred to as structure II. 50 mM **spr** led to the usual diamond-shaped crystals and crystallization was inhibited at **spr** concentrations ≥ 60 mM, suggesting that **sclx₈** – **spr** complexes prevailed under these conditions. This latter observation agrees with the competitor role of **spr**, as evidenced by the NMR experiments (Figure S2).

The use of the dry-coating co-crystallization technique⁴² yielded two crystal forms in the same drop, including an ovoid form which appeared after 20 days (Figure 2, dashed box). This crystal form is referred to as structure III.

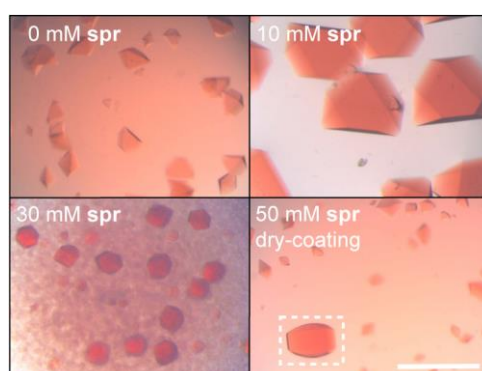


Figure 2. Representative cytc – **sclx₈** co-crystals obtained in the presence of the indicated **spr** concentration. Dry-coating refers to crystals obtained over a layer of **spr** (Methods and Figure S4). The dashed box highlights the ovoid crystal form. Scale bar = 200 μm .

Crystal structure analysis. All of the crystals described here were obtained in similar conditions of ammonium sulfate (~ 2 M), 0.1 M HEPES pH 7.8 and 0.15 M NaCl. X-ray diffraction data were collected at SOLEIL synchrotron. The soaked crystals (50 - 200 mM **spr**) and the co-crystals obtained with 10 or 20 mM **spr** diffracted to 2.2 or 2.3 \AA , which was better than the resolution (2.5 \AA) obtained without **spr** (Tables 1 and S1). All of these structures obtained with **spr** were identical within error. Therefore, only the 50 mM **spr** soak is reported in detail (structure I). The main change compared to the original structure **0** was the presence of **spr** in each of the cavities presented by **sclx₈** in the double cone conformation (Figures 3 and S5). Each of these **spr** also complexes a sulfate anion from the crystallization medium. Interestingly, the solvent-exposed “switch” **sclx₈** was unaffected by the presence of **spr** (Figure S6). This result indicates that the protein – calixarene complex is tighter than the **sclx₈** – **spr** interaction, under these conditions.

Table 1. Crystal structures of cytc – **sclx₈** – **spr** complexes*

Name ^a	Method ^b	PDB id	Res. (Å)	SC ^c (%)	[Building Block] (mM) ^d		
					cytc	sclx ₈	spr
0	-	6rsi	2.5	85	15	45	0
I	Soak	6rsj	2.2	85	15	45	30
II	Co-crystal.	6rsk	2.3	70	30	90	60
III	Dry-coating	6rsl	2.0	70	30	90	120

*All crystals were space group $P4_32_12$ with similar unit cell parameters (Table S1).

^aStructure names **I**, **II**, and **III** correspond to panels **I**, **II**, and **III** in Figures 3-5.

^b**spr** was introduced by soaking, by standard co-crystallization or by dry-coating⁴² co-crystallization.

^cSolvent content estimated in BUSTER, accounting for protein and ligand mass.

^dCalculated based on unit cell volume and the numbers of each building block refined in the model.

Crystals obtained by co-crystallization with **spr** (structures **II** and **III**) had the same space group and similar unit cell parameters as structure **I** (Table S1). However, the asymmetric unit and crystal packing were dramatically altered (Figure 3). The asymmetric units of structures **II** and **III** comprise two cytc and six **sclx₈** molecules. Compared to the original lattice, the protein and calixarene concentrations are doubled. Consequently, the crystalline architectures are less porous (Figures 3 and S7) with solvent contents of 70 % (Table 1).

Figure 4 gives a detailed view of the protein component of the crystal lattices. The original cytc – **sclx₈** crystalline framework (PDB 6gd9)²⁹ is present in all three structures. Structure **III**, is composed of two almost identical copies of the framework from structure **I**. The second copy can be described either as a rotation or as a translation relative to the original framework. Patterson map analysis was used to test the validity of the lattice. A strong off-origin peak in the data for structure **III** was completely absent from structures **0**, **I** and **II** (Figure S8 and Table S2). An additional confirmation was obtained by comparing the R-factors for the integrated intensities for structure **I** against the models for structures **I** or **III** (aligned *via* chain A). The R-factors (highest resolution range in parenthesis) were 0.46 (0.44) for model **III** compared to 0.18 (0.23) for the correct model **I**, proving that the additional lattice does not occur in structures **0** or **I**. In structure **II** the second framework is arranged differently. Here, the second cytc monomer is displaced by ~10 Å and at an angle of ~20° (Figure S9) relative to its position in structure **III**. Concomitantly, a **sclx₈**-mediated crystal contact is lost and replaced by a protein – protein interface. Overall, these results are consistent with the assumption that the porous framework could be augmented by additional building blocks. Framework duplication has been reported recently for Pd-mediated coordination cages.⁴³

The solvent channels in structures **I**, **II** and **III** were characterized computationally.⁴⁴ Crystalline framework **I** can accommodate spheres of ~5.5 nm diameter. In structures **II** and **III** the cavities are partially filled by additional cytc – **sclx₈** building blocks. Nevertheless, the remaining

voids can accommodate spheres of ~3 nm diameter. These cavities are sufficiently large to permit the addition of yet further building blocks and / or to modulate their orientation.

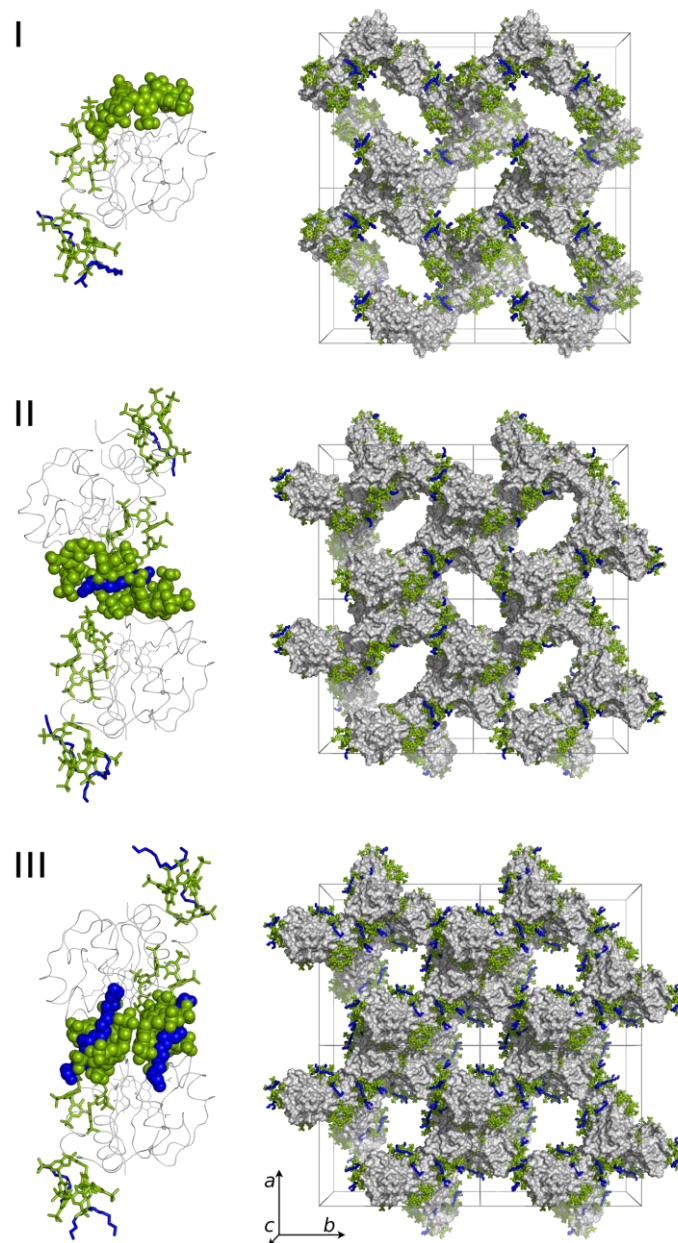


Figure 3. The asymmetric unit and crystal packing in structures **I**, **II** and **III** with *cytc*, **sclx₈** and **spr** depicted in grey, green, and blue, respectively. The asymmetric units are oriented identically (aligned *via* chain A). The “switch” **sclx₈** and associated **spr** are displayed in spacefill, other ligands are in stick. The crystal packing shows 4 unit cells oriented identically with unit cell axes $a = b \approx 10$ nm. Note the high porosity due to nm scale solvent-filled voids.

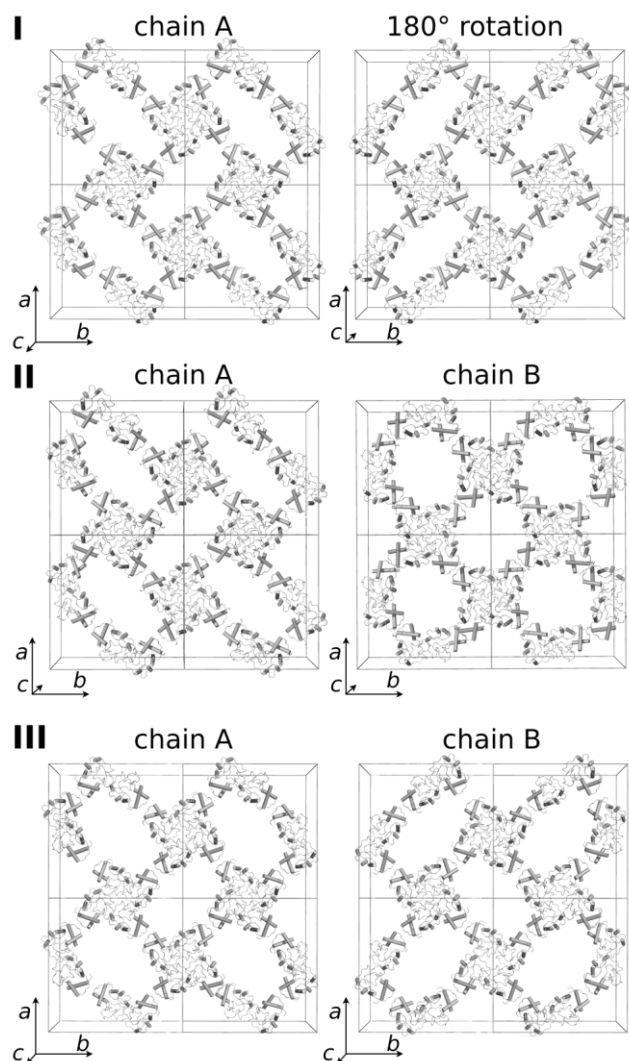


Figure 4. Analysis of the crystalline frameworks in structures **I**, **II** and **III**. The packing of structure **I** is shown in two orientations. For structures **II** and **III** the packing was deconstructed to show separately the architectures of protein chains A and B. The rotation of structure **I** is equivalent to chain B in structure **III**. Only the protein components are depicted.

The “switch” calixarene, spr complexation and framework selection. Architectures **I**, **II** and **III** depend on **sclx₈**, which mediates most of the crystal contacts. In all three structures two of the calixarenes are conserved (Figures 1 and S5). In contrast, the “switch” **sclx₈** adopts a different conformation and binding mode in each structure, and contributes to the incorporation of a second **cytc** unit in architectures **II** and **III** (Figure 5). In each case, two “switch” calixarenes are close-packed and bound to **spr**. Therefore, complex formation between **spr** and the “switch” calixarene appears to contribute to modulating the crystal architecture. Figures 5 and S6 provide detailed views of the

“switch” site in all three structures. The interaction energies of this **sclx₈** in each structure were investigated by DFT calculations. Table S3 lists the key interactions and their respective energies.

In structures **0** and **I**, one face of the “switch” calixarene is bound to protein while the other face is solvent exposed (Figure 5). Four key residues, R13, K72, K73 and K86 bind to **sclx₈**, which masks 530 Å² of the *cytc* surface. The calculated interaction energy for this site is -89 kcal.mol⁻¹. Crystal soaking with **spr** was expected to alter this ligand but there was no evidence of significant changes in the electron density map. In structure **II**, the “switch” **sclx₈** adopts a conformation that is intermediate to the double cone and the pleated loop. This partially-folded **sclx₈** yields a smaller interface area, masking 410 Å² of *cytc*. B-factor analysis and DFT calculations suggest that this **sclx₈** is the least stable of structures **I** - **III** (Tables S3 and S4). The rearranged protein – calixarene interface no longer involves R13 and the interaction with K86 is significantly weakened. However, an interaction at K79 contributes to stabilizing the interface. The calculated energy between the “switch” **sclx₈** and *cytc* in structure **II** is -66 kcal.mol⁻¹. At this interface one molecule of **spr**, in an extended conformation, is sandwiched between two calixarenes (See composite omit map, Figure S6). The tetracationic **spr** helps to glue together the two calixarenes, resulting in an overall interaction energy of -99 kcal.mol⁻¹. It can be concluded that co-crystallization with **spr** enabled the construction of these extra laterals in the framework.

In structure **III**, again a dimeric calixarene assembly occurs at the “switch” site. Here, the calixarenes adopt a pronounced double cone conformation and dimerization occurs through a π-π stack^{21,22} of one phenol unit from each ligand (Figure 5). Each **sclx₈** covers 280 Å² of one protein at key residues R13, K86 and K87 and 250 Å² of the second protein at key residues N70, K72 and K73. The interaction energy for this binding site was calculated at -74 kcal.mol⁻¹. Four **spr** were modelled at this site, one in each of the calixarene cavities. The **spr** are well defined, with clear electron density and low B factors (Table S4, Figure S6) and strongly stabilize each **sclx₈**, leading to an overall interaction energy of -184 kcal.mol⁻¹, which is almost 2-fold more stable than the corresponding site in structure **II**.

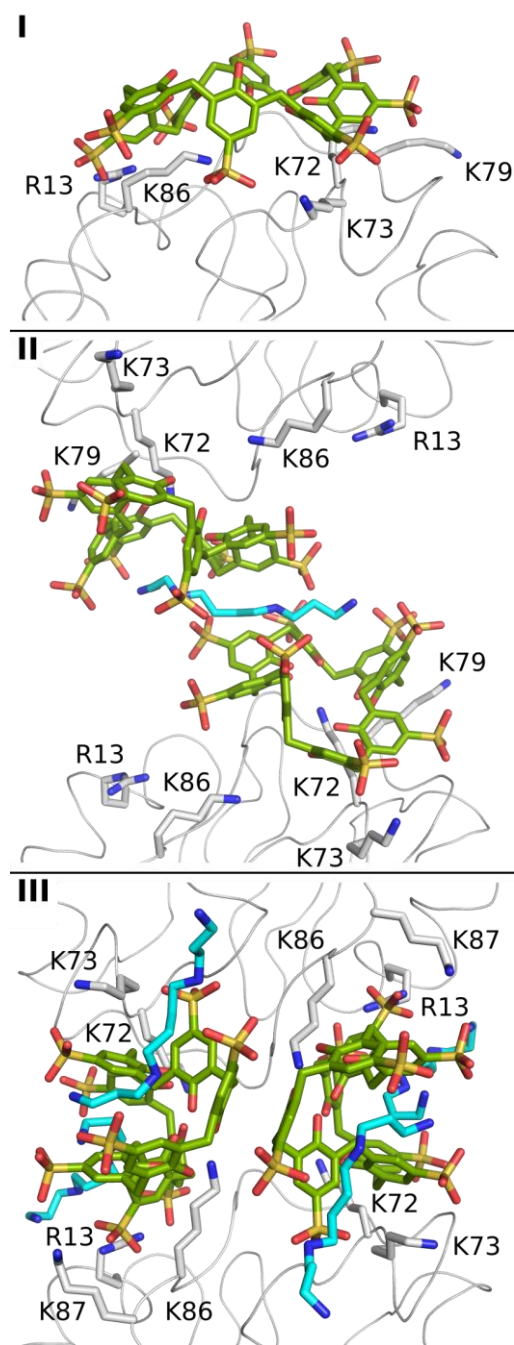


Figure 5. Conformation change and interaction modulation of the “switch” $sclx_8$ in structures I, II and III. The “switch” $sclx_8$, spr and residues of interest are shown as sticks in each structure. Note the solvent exposed face of $sclx_8$ in structure I. spr is coloured cyan and navy for carbon and nitrogen, respectively.

Discussion

Motivated by the possibilities of host – guest supramolecular chemistry we tested the effect of **spr** on a highly porous cytc – **sclx₈** crystalline framework (PDB 6gd9). A simple soaking experiment verified the possibility to plug the cavities of **sclx₈** with cationic **spr**. More exciting results were obtained from co-crystallization experiments that resulted in duplicated frameworks with distinct structures (Table 1, Figures 3 and 5). Surprisingly, larger and better-diffracting crystals with an identical composition were obtained at relatively low **spr** concentrations (10 or 20 mM). In this situation, **spr** – **sclx₈** complexation may improve crystal quality by stabilizing the crystal contacts that are mediated by the conserved **sclx₈** in the double cone conformation (Figures 1 and S5).

Higher equivalents of **spr** during co-crystallization resulted in two different crystal-packing arrangements that involve double the number of cytc and **sclx₈** molecules with respect to the original architecture (Table 1). The incorporation of an additional cytc – **sclx₈** building block necessitates the formation of additional interfaces. In structure **II**, an extra crystal packing interface occurs with **spr** sandwiched between two “switch” calixarenes, which in turn mediate protein – protein packing (Figure 5). Apparently, the effector alters the “switch” calixarene conformation and facilitates close packing of two **sclx₈**. This architecture appears to be an intermediate state between structures **I** and **III**, as reflected by high B-factors of the “switch” **sclx₈** (Table S4) and by the loss of a crystal packing contact (Figure S9).

In structure **III** the “switch” calixarene forms a double cone with one **spr** bound in each cavity, supporting a more stable framework compared to structure **II** (Figure 5, Table S3). Here, the dry-coating technique (Figure S4) facilitated slow diffusion of **spr** into the crystallization drop and consequently a shifting equilibrium of **spr** – **sclx₈** complexation was achieved. Assuming that all of the **spr** dissolved in the drop the final **spr:sclx₈** ratio of 2.5 differed greatly to that in structure **II** (0.75, Table S1). The slow crystallization process (20 days) as well as the shifting (and eventually higher) effector:ligand ratio enabled selection of structure **III**, possibly *via* a kinetic trap.⁴⁵ In contrast, standard co-crystallization at a **spr:sclx₈** ratio ≥ 3 , inhibited crystal growth. The conformation change of the “switch” **sclx₈** from extended to double cone, and host – guest chemistry with **spr**, gives rise to an alternative packing arrangement with the second building block. Interestingly, in all 3 structures the di-lysine motif K72-K73 is pivotal to binding the “switch” calixarene (Figure 5 and Table S3). The structural similarity of this motif and **spr** is noteworthy (Figure S1).

The crystalline framework of structure **III** is composed of two copies of the original architecture related by a translation or by a rotation. This duplicated architecture of interlocking frameworks is enabled by the high-symmetry crystal contacts at the “switch” **sclx₈**, which appears

to dictate the position and orientation of the extra building blocks. The addition of a second set of building blocks leads to decreased crystal porosity. Nevertheless, the solvent content of structures **II** and **III** remains high at 70 %. The 3 nm pores suggest that diffusion of free cytc remains possible and that further modification of crystal porosity could be achieved.

Questions remain concerning the nature of the cytc – **sclx₈** – **spr** interactions. In particular, the contribution of charge – charge interactions and the hydrophobic effect at ~2 M ammonium sulfate requires further investigation. Although the apparent net charge of cytc is close to zero (due to sulfate-binding⁴⁶), lysine and arginine residues still play key roles in complexing the anionic **sclx₈**. And **spr** appears to eliminate charge repulsion between adjacent calixarenes in the framework (Figure 5).

Conclusions

Ligand-mediated protein assembly is emerging as a viable strategy for the construction of porous, functional materials.^{12,14,17,29,47} The relatively large (~1.5 kDa) and flexible **sclx₈** presents interesting properties in this regard. By adopting different conformations, **sclx₈** masks the protein surface to varying degrees and provides a relatively homogeneous scaffold for assembly.^{29,30} In addition to complexation with the protein we have shown that host – guest interactions between **sclx₈** and the small biomolecule **spr** result in altered protein assemblies. This phenomenon is supported by the structural similarity between **spr** and the di-lysine motif. Interestingly, all 3 structures involve K72-K73 in binding the “switch” **sclx₈**.

The combination of cytc and excess **sclx₈** induces a highly porous framework with no protein-protein contacts (Figure 1).²⁹ Framework elaboration was achieved by co-crystallization with the effector **spr** yielding biosupramolecular ternary composites of varying stoichiometry (Figure 3 and Table 1). The incorporation of additional blocks appears to rely on **spr** acting as either a supramolecular bridging agent or cavity stabilizer (Figure 5). Previously, we observed calixarene stabilization by complexation with PEG fragments.^{21,30} **spr** contributes to modulating the “switch” conformation, which in turn impacts the crystal architecture. Structure **III** appears to be the most stable configuration with 4 additional **spr** molecules locking the “switch” site. Additional building blocks are accommodated as extra pillars in the framework, leading to a duplication of the framework and a consequent reduction in porosity.

The prospects for protein crystal engineering *via* auxiliary supramolecular interactions are apparent. The combination of **sclx₈** with **spr**, a classic supramolecular building block with a small and relatively simple effector, is a starting point. Alternative effectors such as enzyme substrates or drugs may find application in functional materials.

Methods

Materials. ^{15}N -labelled and unlabelled *Saccharomyces cerevisiae* cytc (C102T) were produced as described.^{20,48} Solutions of **sclx₈** (TCI Chemicals) or **spr** (Sigma Aldrich) were prepared in water and the pH was adjusted to 6.0 using NaOH.

NMR spectroscopy. ^1H - ^{15}N HSQC spectra were acquired on 50 μM ^{15}N -labelled cytc in 20 mM potassium phosphate, 50 mM NaCl, 1 mM ascorbate, pH 6.0 at 30 °C with a 600 MHz Varian spectrometer and a HCN cold probe.²⁰ Titrations were performed with cytc – **sclx₈** mixtures at 1 or 3 eq. calixarene and 1 - 16 eq. of **spr**. The sample pH was verified to be constant throughout the titration. Spectra were acquired with 8 scans and 64 increments.

Crystallization and X-ray data collection. Co-crystallization experiments were performed by the hanging drop vapour diffusion method at 20 °C. Protein – calixarene mixtures were tested at 2 mM cytc and 20 - 50 mM **sclx₈**. Crystallization drops were prepared by mixing 2 μl of protein – ligand solution with 1 μl of the reservoir solution that contained 1.8 – 2.4 M ammonium sulfate, 0.1 M HEPES pH 7.8 and 0.15 M NaCl. Crystals were cryo-cooled in liquid nitrogen in their respective crystallization condition supplemented with 25 % glycerol. For the soaking experiments, the cryo-protection solution was supplemented with 50 - 200 mM **spr** and crystals were soaked for up to 5 minutes. Dry-coating crystallization was performed as described.⁴² A 2 μl drop of 50 mM **spr** was applied to a siliconized glass coverslip and evaporated to dryness. The crystallization drop was placed directly on the dry-coated **spr**. Diffraction data were collected on PROXIMA-2A at SOLEIL synchrotron (France) using ϕ scans of 0.1° over 360° and an Eiger X 9M detector.

Structure determination. Diffraction frames were processed in AUTOPROC,⁴⁹ data were integrated in XDS⁵⁰ and the integrated intensities were scaled and merged in AIMLESS⁵¹ and POINTLESS,⁵² as implemented in CCP4. The analysis of the Patterson function using PHENIX XTRIAGE revealed a significant off-origin peak indicating pseudo-translational symmetry in the intensities from structure **III**. Molecular replacement was performed with PHASER⁵³ using PDB 6gd9 as the search model. The models were optimized through iterative rounds of model building in COOT⁵⁴ and refinement in BUSTER⁵⁵ for structures **0**, **I**, **II** and PHENIX⁵⁶ for structure **III**. At all stages of the refinement, translation-liberation-screw-rotation (TLS) and automatic water placement were applied. Data collection and refinement statistics are reported in Table S1. Structures and

associated structure factor amplitudes were deposited in the Protein Data Bank after validation with MolProbity.⁵⁷ The PDB codes are reported in Tables 1 and S1.

Characterization of porous crystalline frameworks. Structures **I**, **II** and **III** were analysed by using MAP_CHANNELS,⁴⁴ to determine the maximum pore diameters.

DFT-based interaction energies. Starting from the X-ray structures, DFT calculations were performed to estimate the binding energies of the “switch” calixarene (Table S3). Minimization of the structures was performed with 5,000 steps of steepest descent followed by 5,000 steps of conjugated gradients, in the Amber18 suite of programs⁵⁸ with the ff14SB force field.⁵⁹ Parameters for **spr** were taken from an earlier study⁵⁷ and **sclx**₈ point charges were computed with the RESP protocol.⁶¹ The temperature was held constant with a Langevin thermostat, with a collision frequency of 1 ps⁻¹. A first 100 ps equilibration run was performed in NPT conditions, followed by a second run in NVT conditions. Finally, a 10 ns simulation was executed at constant pressure using a Berendsen thermostat. Final geometries were obtained after QM/MM optimization using in-house code that couples Gaussian16 to TinkerHP,⁶² using the B3LYP-D3BJ density functionals with the 6-31G(d,p) basis set augmented by diffuse functions for the sulfonate oxygens. This protocol provides final geometries with minimal deviations compared to the X-ray structures. In structure **II** chains A and B have a C^α RMSD of 0.20 Å. Separate DFT calculations were performed for each chain and averaged. In structure **III** chains A and B have a C^α RMSD of 0.07 Å, and were assumed to be identical. Interaction energies are reported for chain A only.

Acknowledgements

This research was supported by NUI Galway, the SYSPROD project (AXELERA Pôle de Compétitivité) and Science Foundation Ireland (grant 13/CDA/2168 to PBC). We thank SOLEIL synchrotron (Paris) for beam time allocation, and the staff at beam line PROXIMA-2A for their assistance with data collection.

Supporting Information

The Supporting Information is available free of charge on the ACS Publications website at DOI: ...

9 figures and 4 tables detailing: similarity of di-lysine and **spr**; NMR competition study; overlay of structures **0** and PDB 6gd9; dry-coating co-crystallization; X-ray data collection, processing and refinement statistics; composite omit maps; crystal packing in structures **I**, **II** and **III**; Patterson maps; highest off-origin Patterson peaks; DFT energies for the “switch” site; average B-factors for **sclx₈**.

References

1. Margolin, A. L.; Navia, M. A. Protein Crystals as Novel Catalytic Materials. *Angew. Chem. Int. Ed.* **2001**, *40*, 2204–2222.
2. Ueno, T. Porous Protein Crystals as Reaction Vessels. *Chem. Eur. J.* **2013**, *19*, 9096–9102.
3. Hudalla, G. A.; Sun, T.; Gasiorowski, J. Z.; Han, H.; Tian, Y. F.; Chong, A. S.; Collier, J. H. Graded Assembly of Multiple Proteins into Supramolecular Nanomaterials. *Nat Mater.* **2014**, *13*, 829–836.
4. Sun, H. C.; Miao, L.; Li, J. X.; Fu, S.; An, G.; Si, C. Y.; Dong, Z. Y.; Luo, Q.; Yu, S. J.; Xu, J. Y.; Liu, J. Self-Assembly of Cricoid Proteins Induced by "Soft Nanoparticles": An Approach to Design Multienzyme-Cooperative Antioxidative Systems. *ACS Nano* **2015**, *9*, 5461–5469.
5. Webber, M. J.; Appel, E. A.; Meijer, E. W.; Langer, R. Supramolecular Biomaterials. *Nat. Mater.* **2016**, *15*, 13–26.
6. Bai, Y.; Luo, Q.; Zhang, W.; Miao, L.; Xu, J.; Li, H.; Liu, J. Highly Ordered Protein Nanorings Designed by Accurate Control of Glutathione S-Transferase Self-Assembly. *J. Am. Chem. Soc.* **2013**, *135*, 10966–10969.
7. Lai, Y. T.; Reading, E.; Hura, G. L.; Tsai, K. L.; Laganowsky, A.; Asturias, F. J.; Tainer, J. A.; Robinson, C. V.; Yeates, T. O. Structure of a Designed Protein Cage that Self-Assembles into a Highly Porous Cube. *Nat. Chem.* **2014**, *6*, 1065–1071.
8. Brasch, M.; Putri, R. M.; de Ruiter, M. V.; Luque, D.; Koay, M. S. T.; Castón, J. R.; Cornelissen, J. J. L. M. Assembling Enzymatic Cascade Pathways inside Virus-Based Nanocages Using Dual-Tasking Nucleic Acid Tags. *J. Am. Chem. Soc.* **2017**, *139*, 1512–1519.
9. Dang, S.; Zhu, Q.; Xu, Q. Nanomaterials Derived from Metal-Organic Frameworks. *Nat. Rev. Mater.* **2017**, *3*, 17075.
10. Hsia, Y.; Bale, J. B.; Gonen, S.; Shi, D.; Sheffler, W.; Fong, K. K.; Nattermann, U.; Xu, C.; Huang, P.; Ravichandran, R.; Yi, S.; Davis, T. N.; Gonen, T.; King, N. P.; Baker, D. Design of a Hyperstable 60-Subunit Protein Icosahedron. *Nature* **2016**, *535*, 136–139.
11. Bale, J. B.; Gonen, S.; Liu, Y.; Sheffler, W.; Ellis, D.; Thomas, C.; Cascio, D.; Yeates, T. O.; Gonen, T.; King, N. P.; Baker, D. Accurate Design of Megadalton-Scale Two-Component Icosahedral Protein Complexes. *Science* **2016**, *353*, 389–394.
12. Beyeh, N. K.; Nonappa; Liljeström, V.; Mikkilä, J.; Korpi, A.; Bochicchio, D.; Pavan, G. M.; Ikkala, O.; Ras, R. H. A.; Kostianen, M. A. Crystalline Cyclophane-Protein Cage Frameworks. *ACS Nano* **2018**, *12*, 8029–8036.
13. Malay, A. D.; Miyazaki, N.; Biela, A.; Chakraborti, S.; Majsterkiewicz, K.; Stupka, I.; Kaplan, C. S.; Kowalczyk, A.; Piette, B. M. A. G.; Hochberg, G. K. A.; Wu, D.; Wrobel, T. P.; Fineberg, A.;

- Kushwah, M. S.; Kelemen, M.; Vavpetič, P.; Pelicon, P.; Kukura, P.; Benesch, J. L. P.; Iwasaki, K.; *et al.* An Ultra-Stable Gold-Coordinated Protein Cage Displaying Reversible Assembly. *Nature* **2019**, *569*, 438–442.
14. Sakai, F.; Yang, G.; Weiss, M. S.; Liu, Y.; Chen, G.; Jiang, M. Protein Crystalline Frameworks with Controllable Interpenetration Directed by Dual Supramolecular Interactions. *Nat. Commun.* **2014**, *21*, 5:4634.
 15. Suzuki, Y.; Cardone, G.; Restrepo, D.; Zavattieri, P. D.; Baker, T. S.; Tezcan, F. A. Self-Assembly of Coherently Dynamic, Auxetic, Two-Dimensional Protein Crystals. *Nature* **2016**, *533*, 369–373.
 16. Abe, S.; Tabe, H.; Ijiri, H.; Yamashita, K.; Hirata, K.; Atsumi, K.; Shimoi, T.; Akai, M.; Mori, H.; Kitagawa, S.; Ueno, T. Crystal Engineering of Self-Assembled Porous Protein Materials in Living Cells. *ACS Nano* **2017**, *11*, 2410–2419.
 17. Van Dun, S.; Ottmann, C.; Milroy, L. G.; Brunsveld, L. Supramolecular Chemistry Targeting Proteins. *J. Am. Chem. Soc.* **2017**, *139*, 13960–13968.
 18. Maita, N. Crystal Structure Determination of Ubiquitin by Fusion to a Protein That Forms a Highly Porous Crystal Lattice. *J. Am. Chem. Soc.* **2018**, *140*, 13546–13549.
 19. Nguyen, T. K.; Negishi, H.; Abe, S.; Ueno, T. Construction of Supramolecular Nanotubes from Protein Crystals. *Chem. Sci.* **2018**, *10*, 1046–1051.
 20. McGovern, R. E.; Fernandes, H.; Khan, A. R.; Power, N. P.; Crowley, P. B. Protein Camouflage in Cytochrome *c*-Calixarene Complexes. *Nat. Chem.* **2012**, *4*, 527–533.
 21. McGovern, R. E.; McCarthy, A. A.; Crowley, P. B. Protein Assembly Mediated by Sulfonatocalix[4]arene. *Chem. Commun.* **2014**, *50*, 10412–10415.
 22. Rennie, M. L.; Doolan, A. M.; Raston, C. L.; Crowley, P. B. Protein Dimerization on a Phosphonated Calix[6]arene Disc. *Angew. Chem. Int. Ed.* **2017**, *56*, 5517–5521.
 23. Jewginski, M.; Granier, T.; Langlois d'Estaintot, B.; Fischer, L.; Mackereth, C. D.; Huc, I. Self-Assembled Protein-Aromatic Foldamer Complexes with 2:3 and 2:2:1 Stoichiometries. *J. Am. Chem. Soc.* **2017**, *139*, 2928–2931.
 24. Doolan, A. M.; Rennie, M. L.; Crowley, P. B. Protein Recognition by Functionalized Sulfonatocalix[4]arenes. *Chem. Eur. J.* **2018**, *24*, 984–991.
 25. Engilberge, S.; Riobé, F.; Wagner, T.; Di Pietro, S.; Breyton, C.; Franzetti, B.; Shima, S.; Girard, E.; Dumont, E.; Maury, O. Unveiling the Binding Modes of the Crystallophore, a Terbium-based Nucleating and Phasing Molecular Agent for Protein Crystallography. *Chem. Eur. J.* **2018**, *24*, 9739–9746.
 26. Mac Sweeney, A.; Chambovey, A.; Wicki, M.; Müller, M.; Artico, N.; Lange, R.; Bijelic, A.;

- Breibeck, J.; Rompel, A. The Crystallization Additive Hexatungstotellurate Promotes the Crystallization of the HSP70 Nucleotide Binding Domain into Two Different Crystal Forms. *PLoS One* **2018**, *13*, e0199639.
27. Guagnini, F.; Antonik, P. M.; Rennie, M. L.; O'Byrne, P.; Khan, A. R.; Pinalli, R.; Dalcanale, E.; Crowley, P. B. Cucurbit[7]uril-Dimethyllysine Recognition in a Model Protein. *Angew. Chem. Int. Ed.* **2018**, *57*, 7126–7130.
28. Alex, J. M.; Rennie, M. L.; Volpi, S.; Sansone, F.; Casnati, A.; Crowley, P. B. Phosphonated Calixarene as a “Molecular Glue” for Protein Crystallization. *Cryst. Growth Des.* **2018**, *18*, 2467–2473.
29. Rennie, M. L.; Fox, G. C.; Pérez, J.; Crowley, P. B. Auto-Regulated Protein Assembly on a Supramolecular Scaffold. *Angew. Chem. Int. Ed.* **2018**, *57*, 13764–13769.
30. Alex, J. M.; Rennie, M. L.; Engilberge, S.; Lehoczki, G.; Dorottya, H.; Fizil, A.; Batta, G.; Crowley P. B. Calixarene-Mediated Assembly of a Small Antifungal Protein. *IUCrJ* **2019**, *6*, 238–247.
31. Rennie, M. L.; Crowley, P. B. A Thermodynamic Model of Auto-Regulated Protein Assembly by a Supramolecular Scaffold. *ChemPhysChem.* **2019**, *20*, 1–8.
32. McGovern, R. E.; Feifel, S. C.; Lisdat, F.; Crowley, P. B. Microscale Crystals of Cytochrome c and Calixarene on Electrodes: Interprotein Electron Transfer between Defined Sites. *Angew. Chem. Int. Ed.* **2015**, *54*, 6356–6359.
33. Ciornii, D.; Riedel, M.; Stieger, K. R.; Feifel, S. C.; Hejazi, M.; Lokstein, H.; Zouni, A.; Lisdat, F. Bioelectronic Circuit on a 3D Electrode Architecture: Enzymatic Catalysis Interconnected with Photosystem I. *J. Am. Chem. Soc.* **2017**, *139*, 16478–16481.
34. Perret, F.; Bonnard, V.; Danylyuk, O.; Suwinska, K.; Coleman, A. W. Conformational Extremes in the Supramolecular Assemblies of Para-Sulfonato-Calix[8]arene. *New J. Chem.* **2006**, *30*, 987–990.
35. Makha, M.; Sobolev, A. N.; Raston, C. L. Constructing 2D Porous Material Based on the Assembly of Large Organic Ions: p-Sulfonatocalix[8]arene and Tetraphenylphosphonium Ions. *Chem. Commun.* **2006**, 511-513.
36. Holbrook, S. R.; Sussman, J. L.; Warrant, R. W.; Kim, S. H. Crystal Structure of Yeast Phenylalanine Transfer RNA. II. Structural Features and Functional Implications. *J. Mol. Biol.* **1978**, *123*, 631–660.
37. Kostianen, M. A.; Szilvay, G. R.; Lehtinen, J.; Smith, D. K.; Linder, M. B.; Urtti, A.; Ikkala, O. Precisely Defined Protein-Polymer Conjugates: Construction of Synthetic DNA Binding Domains on Proteins by using Multivalent Dendrons. *ACS Nano* **2007**, *1*, 103–113.
38. Clarke, O. B.; Caputo, A. T.; Hill, A. P.; Vandenberg, J. I.; Smith, B. J.; Gulbis, J. M. Domain

- Reorientation and Rotation of an Intracellular Assembly Regulate Conduction in Kir Potassium Channels. *Cell* **2010**, *141*, 1018–1029.
39. La, D. D.; Malegaonkar, J. N.; Al Kobaisi, M.; Bhosale, R. S.; Bhosale, S. V.; S. V. Bhosale S. V. Spermine-Directed Supramolecular Self-Assembly of Water-Soluble AIE-Active Tetraphenylethylene: Nanobelt, Nanosheet, Globular and Nanotubular Structures. *New J. Chem.*, **2018**, *42*, 15379–15386.
 40. D'Urso, A.; Brancatelli, G.; Hickey, N.; Farnetti, E.; De Zorzi, R.; Bonaccorso, C.; Purrello, R.; Geremia, S. Interactions of a Water-Soluble Calix[4]arene with Spermine: Solution and Solid-State Characterisation. *Supramol. Chem.* **2014**, *28*, 499–505.
 41. Engilberge, S.; Rennie, M. L.; Crowley, P. B. Calixarene Capture of Partially Unfolded Cytochrome *c*. *FEBS Lett.* **2019**, *593*, 2112–2117.
 42. Gelin, M.; Delfosse, M.; Allemand, F.; Hoh, F.; Sallaz-Damaz, Y.; Pirocchi, M.; Bourguet, W.; Ferrer, J. L.; Labesse, G.; Guichou, J. L. Combining Dry Co-Crystallization and *In Situ* Diffraction to Facilitate Ligand Screening by X-ray Crystallography. *Acta Cryst. D* **2015**, *71*, 1777–1787.
 43. Zhu, R.; Regeni, I.; Holstein, J. J.; Dittrich, B.; Simon, M.; Prévost, S.; Gradzielski, M.; Clever, G. H. Catenation and Aggregation of Multi-Cavity Coordination Cages. *Angew. Chem. Int. Ed.* **2018**, *57*, 13652–13656.
 44. Juers, D. H.; Ruffin, J. MAP_CHANNELS: A Computation Tool to Aid in the Visualization and Characterization of Solvent Channels in Macromolecular Crystals. *J. Appl. Cryst.* **2014**, *47*, 2105–2108.
 45. Yan, Y.; Huang, J.; Tang, B. Z. Kinetic Trapping - a Strategy for Directing the Self-Assembly of Unique Functional Nanostructures. *Chem. Commun.* **2016**, *52*, 11870–11884.
 46. Kyne, C.; Jordon, K.; Filoti, D. I.; Laue, T. M.; Crowley, P. B. Protein Charge Determination and Implications for Interactions in Cell Extracts. *Protein Sci.* **2017**, *26*, 258–267.
 47. Kuan, S. L.; Bergamini, F. R. G.; Weil, T. Functional Protein Nanostructures: A Chemical Toolbox. *Chem. Soc. Rev.* **2018**, *47*, 9069–9105.
 48. Volkov, A. N.; Vanwetswinkel, S.; Van de Water, K.; van Nuland N. A. Redox-Dependent Conformational Changes in Eukaryotic Cytochromes Revealed by Paramagnetic NMR Spectroscopy. *J. Biomol. NMR* **2012**, *52*, 245–256.
 49. Vonrhein, C.; Flensburg, C.; Keller, P.; Sharff, A.; Smart, O.; Paciorek, W.; Womack, T.; Bricogne, G. Data Processing and Analysis with the autoPROC Toolbox. *Acta Cryst. D* **2011**, *67*, 293–302.
 50. Kabsch, W. XDS. *Acta Cryst. D* **2010**, *66*, 125–132.

51. Evans, P. R.; Murshudov, G. N. How Good are my Data and What is the Resolution? *Acta Cryst. D* **2013**, *69*, 1204–1214.
52. Evans, P. R. An Introduction to Data Reduction: Space-Group Determination, Scaling and Intensity Statistics. *Acta Cryst. D* **2011**, *67*, 282–292.
53. McCoy, A. J.; Grosse-Kunstleve, R. W.; Adams, P. D.; Winn, M. D.; Storoni, L. C.; Read, R. J. Phaser Crystallographic Software. *J. Appl. Cryst.* **2007**, *40*, 658–674.
54. Emsley, P.; Lohkamp, B.; Scott, W. G.; Cowtan, K. Features and Development of Coot. *Acta Cryst. D* **2010**, *66*, 486–501.
55. Bricogne G.; Blanc E.; Brandl M.; Flensburg C.; Keller P.; Paciorek W.; Roversi P.; Sharff A.; Smart O. S.; Vonrhein C.; Womack T. O. (2017). BUSTER version 2.10.3. Cambridge, United Kingdom: Global Phasing Ltd.
56. Adams, P. D.; Afonine, P. V.; Bunkóczi, G.; Chen, V. B.; Davis, I. W.; Echols, N.; Headd, J. J.; Hung, L. W.; Kapral, G. J.; Grosse-Kunstleve, R. W.; McCoy, A. J.; Moriarty, N. W.; Oeffner, R.; Read, R. J.; Richardson, D. C.; Richardson, J. S.; Terwilliger T. C.; Zwart P. H. PHENIX: A Comprehensive Python-Based System for Macromolecular Structure Solution. *Acta Cryst. D* **2010**, *66*, 213–221.
57. Williams, C. J.; Headd, J. J.; Moriarty, N. W.; Prisant, M. G.; Videau, L. L.; Deis, L. N.; Verma, V.; Keedy, D. A.; Hintze, B. J.; Chen, V. B.; Jain, S.; Lewis, S. M.; Arendall, W. B.; Snoeyink, J.; Adams, P. D.; Lovell, S. C.; Richardson, J. S.; Richardson, D. C. MolProbity: More and Better Reference Data for Improved All-Atom Structure Validation. *Protein Science* **2018**, *27*, 293–315.
58. Case, D. A.; Ben-Shalom, I. Y.; Brozell, S. R.; Cerutti, D. S.; Cheatham, T. E.; Cruzeiro, V. W. D.; Darden, T. A.; Duke, R. E.; Ghoreishi, D.; Gilson, M. K.; Gohlke, H.; Goetz, A. W.; Greene, D.; Harris, R.; Homeyer, N.; Izadi, S.; Kovalenko, A.; Kurtzman, T.; Lee, T. S.; LeGrand, S.; *et al.* (2018), AMBER 2018, University of California, San Francisco.
59. Maier, J. A.; Martinez, C.; Kasavajhala, K.; Wickstrom, L.; Hauser, K. E.; Simmerling, C. ff14SB: Improving the Accuracy of Protein Side Chain and Backbone Parameters from ff99SB. *J. Chem. Theory. Comput.* **2015**, *11*, 3696–3713.
60. Bignon, E.; Chan C. H.; Morell, C.; Monari, A.; Ravanat, J. L.; Dumont, E. Molecular Dynamics Insights into Polyamine-DNA Binding Modes: Implications for Cross-Link Selectivity. *Chem. Eur. J.* **2017**, *52*, 12845–12852.
61. Wang, J.; Cieplak, P.; Kollman, P. A. How Well Does a Restrained Electrostatic Potential (RESP) Model Perform in Calculating Conformational Energies of Organic and Biological Molecules? *J. Comput. Chem.* **2000**, *21*, 1049–1074.

62. Ponder, J. W. (2004). TINKER, Software Tools for Molecular Design, Version 6.3.

Table of Contents Graphic

Framework Composition		
# Building Blocks		
Protein	Macrocycle	Effector
1	3	0
1	3	2
2	6	4
2	6	8

